

# Electron-Spin Beat Susceptibility of Excitons in Semiconductor Quantum Wells

N. H. Kwong, Stefan Schumacher,\* and R. Binder

*College of Optical Sciences, University of Arizona, Tucson, Arizona 85721, USA*

(Received 13 April 2008; revised manuscript received 29 June 2009; published 29 July 2009)

Recent time-resolved differential transmission and Faraday rotation measurements of long-lived electron-spin coherence in quantum wells displayed intriguing parametric dependencies. For their understanding we formulate a microscopic theory of the optical response of a gas of optically incoherent excitons whose constituent electrons retain spin coherence, under a weak magnetic field applied in the quantum well's plane. We define a spin beat susceptibility and evaluate it in linear order of the exciton density. Our results explain the many-body physics underlying the basic features observed in the experimental measurements.

DOI: 10.1103/PhysRevLett.103.056405

PACS numbers: 71.35.Gg, 42.50.Md, 78.20.Ls

Spurred by prospects of applications in spintronics, the long-lived electron-spin coherence of excitations in semiconductor quantum wells has been undergoing intensive investigation [1–3]. Experimentally one of the most direct and convenient ways to study this spin coherence is through the measurement of its effects on the quantum well's optical response. Nonlinear optics techniques such as differential transmission (DT) and Faraday rotation (FR) of optical probes have been used for this purpose [4–7]. Typically, the electron-hole excitation is produced in a pure spin state aligned with the quantum well's growth axis in the presence of a weak magnetic field applied along the well's plane [Voigt geometry, Fig. 1(a)]. Time-resolved DT and FR signals oscillating at the electron-spin Zeeman splitting frequency are then generated by probe pulses at delay times spread over hundreds of picoseconds.

While the decay of the electron-spin signals is by now well understood (for a review, see, e.g., [8]), other fundamental parametric dependencies are still under active investigation. Recent reports on the measurement (DT and FR) and control of electron-spin coherence in a pumped population of excitons [6,7,9] showed intriguing dependencies on probe frequency and intensity, which could reveal important information about the nonlinear optical properties of the electron-spin coherent, but optically incoherent, excitons. The experiments have been interpreted with phenomenological models, but a microscopic theory would provide a more in-depth understanding. The purpose of this Letter is to formulate a general microscopic theory of the nonlinear optical susceptibility of a quantum well which carries a population of electron-spin-coherent excitons. Valid in linear order in both the pumped exciton density and probe field amplitude, the theory clarifies the physics of time-resolved DT and FR spin beats at the low density limit.

Microscopic theories have been extensively developed for the nonlinear response of quantum wells in the ultrafast ( $\leq$  several ps) regime. In conjunction with significant experimental efforts, these theories have established exciton-exciton interactions as the primary mechanism

driving nonlinear optical effects (for recent reviews, see, e.g., [10–12]). In particular, the microscopic processes underlying exciton-spin beats in FR signals in this regime have been discussed [13,14]. But so far a microscopic theory of the nonlinear optics of optically dephased, electron-spin-coherent excitons on the 100 ps time scale is still absent.

We consider specifically the experimental configuration sketched in Fig. 1(a). A circularly polarized, say,  $\sigma = +$ , pump pulse propagating at normal incidence (along the  $z$  axis) and spectrally close to the lowest heavy hole exciton resonance creates an interband polarization in a quantum well at low ambient temperature, e.g., 10 K. Within a time scale  $\tau_R$  ( $< 50$  ps in GaAs at 10 K) after the pumping, the interband polarization partially reradiates and partially dephases and relaxes to yield a population of incoherent heavy hole excitons with a distribution of center-of-mass momentum. The hole spin inside a pumped exciton (initially  $j_z = 3/2$ , corresponding to the absence of a valence

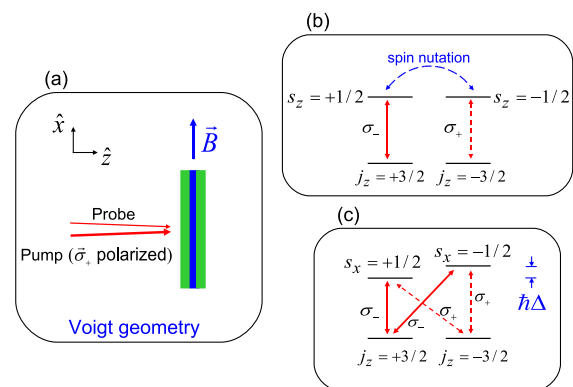


FIG. 1 (color online). (a) Sketch of the Voigt geometry with normal incidence light and a magnetic field  $\mathbf{B}$  in the quantum well plane. (b) Optical selection rules in the  $z$  basis. The  $\mathbf{B}$ -field induced coherence between the electron states in the  $z$  basis is indicated. (c) Optical selection rules using the  $z$  basis for the valence band orbitals and  $x$  basis (eigenstates of magnetic field Hamiltonian) for the conduction band electrons.

electron of spin  $j_z = -3/2$  decoheres also within  $\tau_R$ , while the electron-spin state ( $s_z = -1/2$  initially) stays pure for a long time, e.g., typically hundreds of ps in GaAs quantum wells. A magnetic field applied along an axis (the  $x$  axis) in the plane of the quantum well splits the two degenerate electron-spin states quantized along the  $x$  axis [Fig. 1(c)] and, in the case at hand, drives a coherent oscillation of spin population between the two electron-spin states quantized along the  $z$  axis [Fig. 1(b)]: with the electron created in  $s_z = -1/2$ , the electron-spin density matrix in the  $z$ -axis basis is

$$\hat{\rho}_z^s(t) = \frac{1}{2} \begin{pmatrix} [1 + \cos\Delta(t - t_{\text{pu}})] & i \sin\Delta(t - t_{\text{pu}}) \\ -i \sin\Delta(t - t_{\text{pu}}) & [1 - \cos\Delta(t - t_{\text{pu}})] \end{pmatrix}, \quad (1)$$

where  $\hbar\Delta$  is the Zeeman splitting and  $t_{\text{pu}}$  is the pump time.

Many properties of the exciton population can be described by the one-exciton density matrix  $\langle p_{\mathbf{q}}^{sj\dagger}(t) p_{\mathbf{q}'}^{s'j'}(t) \rangle$  where  $p_{\mathbf{q}}^{sj}$  is the second quantized annihilation operator for a  $1s$  heavy hole exciton with electron-spin  $s$  quantized along the  $\hat{z}$ -axis, hole orbital  $j$ , and center-of-mass in-plane momentum  $\mathbf{q}$  (all momenta in this Letter lie in the quantum well's plane), and  $\langle \cdot \rangle$  denotes an expectation value in a many-exciton state. For times larger than  $\tau_R$ , when the state has decohered with respect to hole spin and momentum, the one-exciton density matrix can to a good approximation be written as an uncorrelated product of matrices in the three state labels:  $\langle p_{\mathbf{q}}^{sj\dagger}(t) p_{\mathbf{q}'}^{s'j'}(t) \rangle = [\hat{\rho}_z^s]_{ss'} (\delta_{jj'}/2) \times \delta_{\mathbf{q}\mathbf{q}'} f(\mathbf{q})$ , where  $f(\mathbf{q})$  is the slowly evolving momentum distribution. The relaxation dynamics of  $f(\mathbf{q})$  has previously been investigated [15]. Based on its findings, we use a model distribution, shown in Fig. 2(e), which is thermal except for a radiative loss correction at low momenta.

Microscopic many-particle theory comes into play when we try to understand the measurement and manipulation of the electron-spin coherence of the exciton population. Suppose a probe pulse  $E_\sigma(t)$ , circularly polarized ( $\sigma =$

+ or -) and centered spectrally at  $\omega$  and temporally at  $t_{\text{pr}}$ , is sent in to measure this coherence. It does so by inducing a  $1s$  heavy hole interband polarization which scatters off the existing electron-spin coherent exciton population. We use real-time Green's functions and diagrammatic perturbation methods (for an account of this formalism see, e.g., [16]) to derive equations of motion for the probe-induced interband polarization in increasing orders of the probe intensity and the preexcited exciton density. These equations are derived with electrons and holes as degrees of freedom. They are then expanded in an exciton basis and restricted to the heavy hole  $1s$  subspace. The resulting equations—our working equations—are driven by various exciton scattering processes and Pauli blocking. (Pauli blocking turns out to be relatively unimportant here.) We illustrate the lowest order scattering processes in Figs. 2(a)–2(d), showing the various electron-spin (in the  $\hat{z}$  basis) combinations explicitly for a ( $\sigma = + \Rightarrow s = -1/2, j = 3/2$ ) probe. In each diagram, the line starting with a cross denotes the  $1s$  interband polarization created by the probe pulse, and the open line a propagating exciton that recombines to give the signal photon. The internal line represents a two-time correlation function of the pumped exciton population  $\langle p_{\mathbf{q}}^{sj\dagger}(t) p_{\mathbf{q}'}^{s'j'}(t') \rangle = \langle p_{\mathbf{q}}^{sj\dagger}(t) p_{\mathbf{q}'}^{s'j'}(t') \rangle \times \exp[i\omega_{\mathbf{q}}(t - t')]$ , where the signs of the electron-spin  $s$  and  $s'$  are marked at the line's two ends, and  $\hbar\omega_{\mathbf{q}}$  is the energy of the exciton with momentum  $\mathbf{q}$ . The scattering matrix [17], or  $T$  matrix (box labeled  $T$ ), is a ladder sum of repeated exciton interactions to all orders. It preserves the hole spins of the scattering excitons individually but allows exchange of electron spins. These (electron and hole) spin conservation rules restrict the contributing electron-spin configurations to those included in Fig. 2, which shows that only the diagonal elements of the electron-spin density matrix,  $[\hat{\rho}_z^s]_{-1/2,-1/2}$  and  $[\hat{\rho}_z^s]_{1/2,1/2}$ , are probed.

The susceptibility for the  $\sigma$ -(circularly)polarized component of the probe is given by  $\chi_\sigma \sim \int dt p_\sigma(t) E_\sigma^*(t)$  where  $p_\sigma(t)$  is the probe-induced interband polarization. The susceptibility depends parametrically on the pump-probe delay time  $\tau = t_{\text{pr}} - t_{\text{pu}}$  and the probe pulse's center frequency  $\omega$ :  $\chi_\sigma = \chi_\sigma(\omega, \tau)$ . It gives the time-resolved FR of an  $x$ -polarized probe and the DT of a  $\sigma$ -polarized probe as [14]  $\theta(\omega, \tau) \sim \text{Re}[\chi_-(\omega, \tau) - \chi_+(\omega, \tau)]$  and  $\Delta T_\sigma(\omega, \tau) \sim -\text{Im}[\chi_\sigma(\omega, \tau)]$ , respectively. We have calculated the susceptibility to linear order in the pump-induced density. Called the third order susceptibility  $\chi_\sigma^{(3)}(\omega, \tau)$ , it can be written in the form

$$\chi_\pm^{(3)}(\omega, \tau) = C(\omega) \pm D_{\text{spin}}(\omega) \cos\Delta\tau. \quad (2)$$

The response signals are similarly parametrized:  $\theta(\omega, \tau) = A_\theta(\omega) \cos\Delta\tau$ ,  $\Delta T_\pm(\omega, \tau) = A(\omega) \pm A_T \cos\Delta\tau$ , with the amplitudes given by  $A_\theta(\omega) \sim -\text{Re}D_{\text{spin}}(\omega)$ ,  $A_T(\omega) \sim -\text{Im}D_{\text{spin}}(\omega)$ , and  $A(\omega) \sim -\text{Re}C(\omega)$ . The probe pulses we use have durations of several ps, which are long compared to the scattering duration (typically  $< 1$  ps in GaAs)

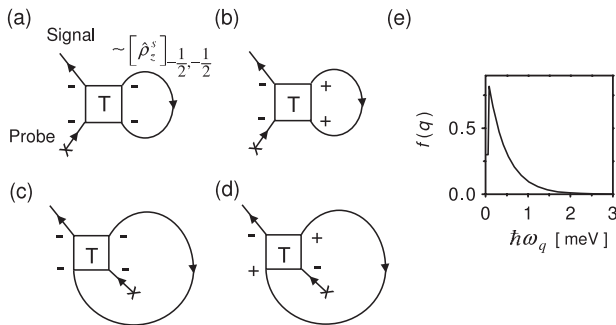


FIG. 2. (a)–(d) Diagrams representing the excitonic scattering contributions to the third order interband polarization. The electron-spin states (+ or -) of the incoming and outgoing excitons of each scattering event in the case of a (+)-polarized probe are marked. See text for the meanings of diagram parts. (e) A model momentum distribution of the relaxed excitons.

but short compared to the spin beat period ( $\sim 70$  ps, corresponding to  $\hbar\Delta \approx 0.06$  meV, in the cited experiments). It is then instructive to approximately treat the probe pulse as a continuous wave in the scattering calculation and the oscillating electron-spin population as frozen within the duration of  $p_\sigma^{(3)}(t)$ . Solving the  $p_\sigma^{(3)}$  equation in this approximation, we obtain the  $\omega$ -dependent coefficients of  $\chi_\sigma^{(3)}$  as [18]

$$C(\omega) \sim - \sum_{\mathbf{q}} \frac{f(\mathbf{q})}{[L(\omega)]^2} \left\{ T_{\mathbf{q}/2, \mathbf{q}/2}^{++}(\Omega_{\mathbf{q}}, \mathbf{q}) + T_{\mathbf{q}/2, -\mathbf{q}/2}^{++}(\Omega_{\mathbf{q}}, \mathbf{q}) \right. \\ \left. + T_{\mathbf{q}/2, \mathbf{q}/2}^{+-}(\Omega_{\mathbf{q}}, \mathbf{q}) - \frac{1}{2} T_{\mathbf{q}/2, -\mathbf{q}/2}^{+-}(\Omega_{\mathbf{q}}, \mathbf{q}) \right. \\ \left. - [\tilde{A}_e^{\text{PSF}}(\mathbf{q}) + \tilde{A}_h^{\text{PSF}}(\mathbf{q})]L(\omega) \right\}, \quad (3)$$

$$D_{\text{spin}}(\omega) \sim - \sum_{\mathbf{q}} \frac{f(\mathbf{q})}{[L(\omega)]^2} \left[ T_{\mathbf{q}/2, \mathbf{q}/2}^{++}(\Omega_{\mathbf{q}}, \mathbf{q}) - T_{\mathbf{q}/2, \mathbf{q}/2}^{+-}(\Omega_{\mathbf{q}}, \mathbf{q}) \right. \\ \left. + \frac{1}{2} T_{\mathbf{q}/2, -\mathbf{q}/2}^{+-}(\Omega_{\mathbf{q}}, \mathbf{q}) - \tilde{A}_e^{\text{PSF}}(\mathbf{q})L(\omega) \right]. \quad (4)$$

Here  $T_{\mathbf{k}_f, \mathbf{k}_i}^{\sigma\sigma'}(\Omega, \mathbf{Q})$  denotes a two-exciton scattering (or  $T$ -matrix) element [17] between an incoming state with relative momentum  $\mathbf{k}_i$  and an outgoing state with relative momentum  $\mathbf{k}_f$ , and  $\hbar\Omega$  and  $\mathbf{Q}$  are the conserved total energy and momentum, respectively. For easier interpretation, we have chosen to parametrize the spin dependence of the  $T$ -matrix elements in the same way as in the coherent regime:  $T^{++}(=T^{--})$  and  $T^{+-}(=T^{-+})$  are, respectively, the  $T$  matrices for copolarized and counterpolarized excitons. For each process both the incoming and outgoing states contain a virtual (probe) exciton with zero momentum and energy  $\hbar\omega$  and a real (pump) exciton with momentum  $\mathbf{q}$  and energy  $\hbar\omega_{\mathbf{q}} = \varepsilon_x + \hbar^2 q^2 / (2M_x)$ ,  $M_x$  being the exciton's mass. These give a total energy of  $\Omega_{\mathbf{q}} = \omega + \omega_{\mathbf{q}}$  and a total momentum of  $\mathbf{q}$ .  $L(\omega) = \hbar\omega - \varepsilon_x + i\gamma$  where  $\gamma$  is the linewidth of the exciton resonance. The phase space filling (PSF) factors are given in terms of the momentum space 1s exciton wave function  $\phi(\mathbf{k})$  by  $\tilde{A}_\alpha^{\text{PSF}}(\mathbf{q}) = \sum_{\mathbf{k}} \phi(\mathbf{k}) |\phi(\mathbf{k}_\alpha)|^2 / \sum_{\mathbf{k}} \phi(\mathbf{k})$ , where  $\mathbf{k}_\alpha = \mathbf{k} - (m_\alpha/M_x)\mathbf{q}$ , with  $\alpha = e, h$ . The  $T$ -matrix elements are calculated by diagonalization of the two-exciton Hamiltonian as explained in [17].

Equation (2) shows a simple dependency to pump-probe polarization configurations: the copolarized (+ pump and + probe) and counterpolarized (+ -) response signals share a common  $\tau$ -independent part but have  $180^\circ$ -out-of-phase spin beat parts. At the same time, Eqs. (3) and (4) show that, even for the copolarized configuration, say, both  $T^{++}$  and  $T^{+-}$  contribute. In particular, biexciton formation, present in  $T^{+-}$ , plays a part in the copolarized channel response. Moreover, Eq. (2) shows that the nonbeat part of the FR of a linearly polarized probe vanishes. These properties follow from our assumption of hole spin thermalization, which produces all four exciton ( $s_z, j_z$ ) spin states in the relaxed exciton population even though the

pump is circularly polarized. These polarization dependencies are in obvious contrast to those of the  $\chi^{(3)}$  susceptibility in ultrafast pump-probe spectroscopy (e.g., [19]), where  $T^{\sigma\sigma'}$  contributes only in the matching ( $\sigma\sigma'$ ) pump-probe polarization channel, yielding distinctly different responses in the (+ +) and (+ -) pump-probe configurations [20]. The combinations of  $T$ -matrix elements in Eqs. (2)–(4) result from superposition of contributions from the processes in Fig. 2. Leaving out common factors, the four diagrams' contributions to  $\chi_+^{(3)}$  are proportional to (a)  $(1 + \cos\Delta\tau)T_{\mathbf{q}/2, \mathbf{q}/2}^{++}$ , (b)  $(1 - \cos\Delta\tau)T_{\mathbf{q}/2, \mathbf{q}/2}^{+-}$ , (c)  $(1 + \cos\Delta\tau)T_{\mathbf{q}/2, -\mathbf{q}/2}^{++}/2$ , (d)  $(1 - \cos\Delta\tau)(T_{\mathbf{q}/2, -\mathbf{q}/2}^{++} - T_{\mathbf{q}/2, -\mathbf{q}/2}^{+-})/2$  [21].

We have calculated  $C(\omega)$  and  $D_{\text{spin}}(\omega)$  for the exciton momentum distribution shown in Fig. 2(e), with an exciton linewidth of  $\gamma = 0.35$  meV and a biexciton dephasing of  $2\gamma$ . In our calculation, the  $p_\sigma^{(3)}(t)$  equation is solved with 4-ps probe pulses, i.e., without assuming the probe to be a continuous wave. The effect of the “continuous-wave” approximation is, however, small so that Eqs. (3) and (4) can be used to interpret the numerical results. Figure 3 shows (a) the spin beat amplitude  $A_T(\omega)$  of the DT of a (+)-polarized (copolarized with the pump) probe, (b) the beat amplitude  $A_\theta(\omega)$  of the FR of a linearly polarized probe, and (c) the nonbeat part  $A(\omega)$  of the DT. The signals' spectral behaviors are basically products of those of the  $T$ -matrix elements and one-exciton Lorentzians  $[L(\omega)]^{-2}$ . The spectra of our finite- $\mathbf{q}$   $T$  matrix here are qualitatively similar to those of the zero- $\mathbf{q}$   $T$  matrix for ultrafast nonlinear optics discussed in [17]. A prominent feature in Fig. 3 is the considerably larger magnitude of the

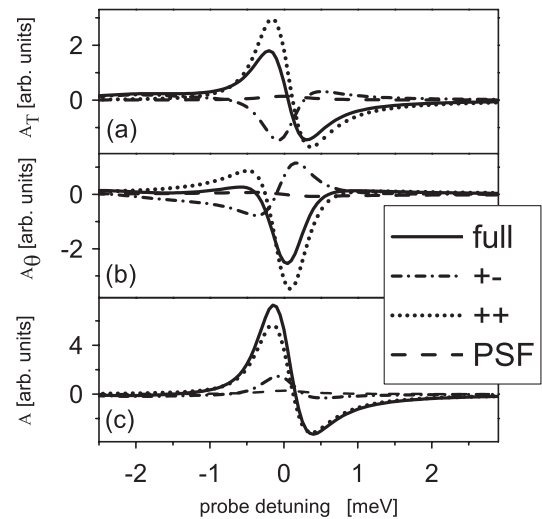


FIG. 3. (a) and (b) The (signed) amplitudes of the electron-spin beat signals of a GaAs quantum well as a function of probe frequency for a (+)-polarized pump: (a) DT of a (+)-polarized probe and (b) FR of a linearly polarized probe. (c) The nonbeat part of the DT. Also shown is the breakdown of each signal into its components: phase space filling (dashed line), exciton scattering  $T^{++}$  (dotted line), and  $T^{+-}$  (dash-dotted line).

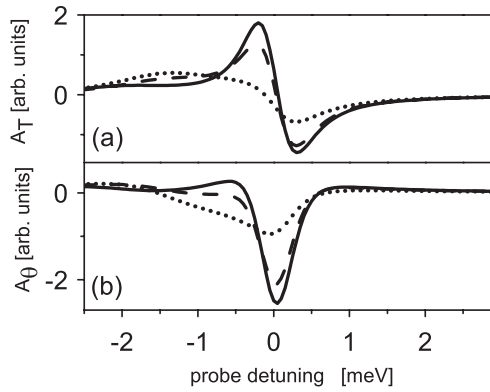


FIG. 4. Sensitivity of the electron-spin beat amplitudes, (a) DT and (b) FR, to variations in the strength and/or resonance energy of the bound biexciton. Solid lines: same as the solid curves in Fig. 3, for which the biexciton binding energy  $\varepsilon_{bx}$  is calculated to be 1.8 meV. Dashed lines:  $\varepsilon_{bx}$  is shifted to 1.3 meV, other components being the same as for the solid curves. Dotted lines:  $\varepsilon_{bx}$  is shifted to 1.3 meV, and biexciton strength is raised by a factor of 1.5.

nonbeat part of the DT signal compared to  $A_T$  and  $A_\theta$ . This can be understood from the breakdown into contributions from various processes, also shown in the figure. For the spin beat amplitudes, the contributions from  $T^{++}$  (dotted lines) and  $T^{+-}$  (dash-dotted lines) largely counteract each other, especially near the exciton resonance ( $\hbar\omega \approx \varepsilon_x$ ). This effect can be expected from the opposite signs with which the two contributions appear in Eq. (4) for  $D_{\text{spin}}(\omega)$ . In contrast, as seen from Eq. (3),  $T^{++}$  and  $T^{+-}$  tend to reinforce each other in  $C(\omega)$ , which also contains an extra  $T_{q/2, -q/2}^{++}$ .

The smallness of  $A_T$  relative to the nonbeating part of the DT signal is in accord with experimental measurements of DT, especially around zero probe detuning [6,7]. The relative phase ( $=180^\circ$ ) between the beats in the DT in the two pump-probe polarization configurations is also confirmed [22]. The  $\omega$  dependence of  $A_\theta$  shown in Fig. 3 also agrees qualitatively with measurements [7]. We note that our theory is essentially parameter free (the input parameters being the electron and hole masses, the background dielectric constant, and environmental dephasings) with a model of a zero-width quantum well with two bands. Bearing this model's limitations in mind, we think the general agreement between our predictions and experiments is sufficient to validate the physical points of our theory. More accurate modeling of the experimental samples, such as including effects of a finite well width and the light hole band, will be done in the future. To get a rough sense of how these modeling advances might change our results, we have repeated our calculations, artificially varying the biexciton energy and strength from their calculated values. These biexciton characteristics are known to depend quite sensitively on the well width. From Fig. 4, one can see the qualitative features of our theory are robust,

but improved sample modeling would be needed for precise predictions.

In summary, we have formulated a microscopic theory, based on exciton interactions, for the electron-spin beat components of differential transmission and Faraday rotation signals of quantum wells carrying a population of dephased, but electron-spin-coherent excitons. This theory explains the basic features of recent experimental results at the limit of low pump-induced density and low probe intensity. The theory will be generalized to higher orders in the probe intensity and to three-pulse configurations [9].

We thank H. Wang, Y. Shen, and S. O'Leary for valuable discussions and JSOP for financial support. S. Schumacher gratefully acknowledges financial support by the DFG (SCHU 1980/3-1).

\*Present address: Physics–School of EPS, Heriot-Watt University, Edinburgh EH14 4AS, UK.

- [1] S. A. Wolf *et al.*, *Science* **294**, 1488 (2001).
- [2] D. D. Awschalom, M. E. Flatté, and N. Samarth, *Sci. Am.* **286**, No. 6, 66 (2002).
- [3] W. H. Lau, J. T. Olesberg, and M. E. Flatté, *Phys. Rev. B* **64**, 161301(R) (2001).
- [4] J. M. Kikkawa and D. D. Awschalom, *Phys. Rev. Lett.* **80**, 4313 (1998).
- [5] N. Samarth, *Solid State Physics* (Elsevier, Amsterdam, 2004), Vol. 58, p. 1.
- [6] P. Palinginis and H. Wang, *Phys. Rev. Lett.* **92**, 037402 (2004).
- [7] Y. Shen *et al.*, *Phys. Rev. B* **72**, 233307 (2005).
- [8] I. Žutić, J. Fabian, and S. das Sarma, *Rev. Mod. Phys.* **76**, 323 (2004).
- [9] Y. Shen, A. M. Goebel, and H. Wang, *Phys. Rev. B* **75**, 045341 (2007).
- [10] D. Chemla and J. Shah, *Nature (London)* **411**, 549 (2001).
- [11] V. M. Axt and T. Kuhn, *Rep. Prog. Phys.* **67**, 433 (2004).
- [12] T. Meier, P. Thomas, and S. W. Koch, *Coherent Semiconductor Optics* (Springer, New York, 2006).
- [13] T. Östreich, K. Schönhammer, and L. J. Sham, *Phys. Rev. Lett.* **75**, 2554 (1995).
- [14] L. Sham, *J. Magn. Magn. Mater.* **200**, 219 (1999).
- [15] C. Piermarocchi *et al.*, *Phys. Rev. B* **53**, 15 834 (1996).
- [16] N. H. Kwong and R. Binder, *Phys. Rev. B* **61**, 8341 (2000).
- [17] R. Takayama *et al.*, *Eur. Phys. J. B* **25**, 445 (2002).
- [18] See EPAPS Document No. E-PRLTAO-103-008933 for technical details on the derivation of Eqs. (3) and (4) in the article. For more information on EPAPS, see <http://www.aip.org/pubservs/epaps.html>.
- [19] R. Takayama *et al.*, *J. Opt. Soc. Am. B* **21**, 2164 (2004).
- [20] C. Sieh *et al.*, *Phys. Rev. Lett.* **82**, 3112 (1999).
- [21] As shown in the momentum dependence, diagrams 2(a) and 2(b) represent forward scattering in the two-exciton center-of-mass frame, while 2(c) and 2(d) represent backward scattering. Since the  $T$  matrix preserves individual hole spin, only those pump-created excitons with hole spin matching that of the probe excitons participate in processes 2(c) and 2(d), hence giving the factors of 1/2.
- [22] Y. Shen and H. Wang (private communication).